

Blue Laser Photopriming: A Method to Enhance Oxidative Phosphorylation Via Stimulation of the Mitochondrial Outer Membrane



Travis Sammons^{1*}, Steve Shanks¹, Kirk Gair², Robert Silverman³ and Stephanie Wautier⁴

¹Erchonia Corporation, Fountain Inn, SC, USA

²Gair Laser Chiropractic, West Covina, CA, USA

³Westchester Integrative Health, White Plains, NY, USA

⁴Wautier Wellness Chiropractic, Marquette, MI, USA

Submission: May 11, 2026; Published: May 21, 2026

*Corresponding author: Travis Sammons, Erchonia Corporation, Fountain Inn, SC, USA

Abstract

Low-level laser therapy (LLLT) is recognized for stimulating mitochondrial function and promoting cellular repair through targeted photochemical activation. This original article introduces blue laser photopriming, a novel concept in LLLT whereby brief exposure to blue laser light (approximately 450 nm) activates the mitochondrial outer membrane via the protein mitoNEET (CISD1), optimizing subsequent laser stimulation of the electron transport chain (ETC). Evidence from molecular, biochemical, and clinical investigations demonstrates that blue laser photopriming enhances oxidative phosphorylation, improves redox balance, and supports more efficient ATP synthesis. This article integrates mechanistic insights and data, proposing a new framework for wavelength-sequenced mitochondrial modulation. These findings position blue laser photopriming as a clinically relevant upstream intervention to enhance the efficacy of conventional LLLT.

Keywords: Low-Level Laser Therapy; Photobiomodulation; Blue Laser; MitoNEET; CISD1; Mitochondrial Outer Membrane; Iron-Sulfur Clusters; Oxidative Phosphorylation; Redox Homeostasis; Photopriming

Abbreviations: ATP: Adenosine Triphosphate; CAT: Catalase; CCO: Cytochrome C Oxidase; CI: Confidence Interval; CISD1: CDGSH Iron Sulfur Domain 1; ETC: Electron Transport Chain; GSH: Glutathione; IF/IHC: Immunofluorescence/Immunohistochemistry; IP+WB: Immunoprecipitation-Coupled Western Blot; LLLT: Low-Level Laser Therapy; L/P: Lactate/Pyruvate; MS: Mass Spectrometry; NIR: Near-Infrared; OMM: Outer Mitochondrial Membrane; OXPHOS: Oxidative Phosphorylation; RBC: Red Blood Cell; ROM: Range Of Motion; ROS: Reactive Oxygen Species; SOD: Superoxide Dismutase; VAS: Visual Analog Scale; WB: Western blot

Introduction

Low-level laser therapy (LLLT) utilizes specific wavelengths of non-thermal light to modulate cellular function through targeted interactions with mitochondrial chromophores [1,2]. The absorbed photons stimulate the electron transport chain (ETC), enhancing mitochondrial respiration and adenosine triphosphate (ATP) synthesis through oxidative phosphorylation (OXPHOS). Historically, the primary focus has been on the interaction between red and near-infrared (NIR) wavelengths and cytochrome c oxidase (CCO, Complex IV), the terminal enzyme of the ETC and the most extensively characterized photoreceptor in LLLT research [2,3].

Emerging evidence highlights the role of the mitochondrial outer membrane as a critical upstream regulator of LLLT efficacy. Specifically, the outer-membrane protein mitoNEET (CISD1) has been identified as a blue wavelength-responsive site that governs mitochondrial readiness [4,5] for oxidative metabolism. Impaired function of this regulatory protein may underlie the diminished or plateaued photobiological response observed in some tissues or pathological conditions during conventional laser treatment. The concept of blue laser photopriming introduces a preparatory photochemical phase that restores outer-membrane function, setting the stage for more effective downstream biomodulation.

The purpose of this article is to integrate mechanistic, molecular, biochemical, and clinical evidence supporting blue laser photoprimering as an upstream mitochondrial outer-membrane intervention that may enhance subsequent red-light LLLT response.

Mechanisms of conventional LLLT

Published data demonstrate that different wavelengths of light drive wavelength-dependent activation of specific ETC complexes, with each spectral range engaging distinct chromophores at characteristic positions along the respiratory chain.

- **Violet Light (~400-430 nm): Early-Chain Electron Entry (Complexes I and II)**

Violet wavelengths carry photon energies of approximately 2.9-3.1 eV, sufficient to influence the flavin-containing enzymes that govern the initial segments of the ETC. At Complex I (NADH dehydrogenase), experimental *in vitro* studies show that high-energy blue/violet photons modulate the redox states of FMN and Fe-S clusters, increasing NADH oxidation and accelerating electron injection into the ubiquinone pool [3,6]. Complex II (succinate dehydrogenase), the only ETC complex directly linked to the TCA cycle, contains chromophores-FAD and heme b-that exhibit absorption shoulders in the 400-450 nm region [3]. Violet light exposure has been shown to enhance succinate turnover and reinforce a second electron-entry pathway that operates independently of NADH, broadening the substrate base available for downstream electron flow and supporting overall respiratory chain throughput.

- **Green Light (~520-540 nm): Mid-Chain Optimization (Complex III)**

Green wavelengths interact with chromophores present in cytochrome bc₁ (Complex III), particularly cytochrome b and the Rieske iron-sulfur protein. Absorption in the green spectral region has been associated with improvements in the Q cycle-the bifurcation mechanism by which electrons are split and directed toward cytochrome c-potentially increasing the efficiency of electron transfer between the early-entry complexes and Complex IV [6]. Complex III is also a major physiological source of superoxide, particularly when upstream mitochondrial membrane potential ($\Delta\psi$ -m) becomes excessively elevated [6]. Photostimulation around 530 nm appears to improve Q-cycle coupling efficiency, reducing premature electron escape and mitochondrial reactive oxygen species (ROS) generation while simultaneously stabilizing the redox state of coenzyme Q and smoothing electron transfer kinetics across the mid-chain interface between Complexes I/II and IV.

- **Red and Near-Infrared Light (630-850 nm): Terminal Oxidase Activation (Complex IV)**

The most extensively characterized photobiological mechanism in LLLT is the absorption of red and NIR wavelengths

by cytochrome c oxidase (CCO, Complex IV), which contains copper and heme a/a₃ centers with peak absorption in this spectral region [1-3]. Photobiomodulation at these wavelengths promotes conformational states that increase CCO affinity for molecular oxygen and accelerate its four-electron reduction to water, while simultaneously displacing inhibitory nitric oxide (NO) bound to the heme-copper binuclear center to restore electron flux [2,3]. These photochemical events drive increased proton translocation across the inner mitochondrial membrane, elevating $\Delta\psi$ -m and directly augmenting the electrochemical gradient that powers ATP synthase (Complex V), resulting in enhanced cellular energy output.

Outer-membrane readiness as an upstream regulatory constraint

While the wavelength-specific interactions described above establish a well-characterized framework for inner-membrane photostimulation, this model implicitly assumes that the mitochondrion is in an optimal state of readiness to receive and respond to photonic input. Emerging evidence suggests this assumption does not always hold. The outer mitochondrial membrane (OMM) functions as a critical upstream regulatory interface-coordinating metabolite exchange, iron-sulfur cluster transfer, and redox signaling-before any photon reaches the inner membrane. When OMM function is compromised, as may occur in chronic disease, oxidative stress, or pathological downregulation of key regulatory proteins, the bioenergetic response to conventional LLLT may be attenuated or plateaued regardless of the wavelength applied. The following section examines the molecular basis of this upstream constraint through the lens of mitoNEET (CISD1), an outer-membrane redox regulator identified as a blue wavelength-responsive target capable of restoring OMM functional readiness prior to inner-membrane photostimulation (Figure 1).

MitoNEET (CISD1): Structure, functions, and context-dependent role

The outer mitochondrial membrane (OMM) is a dynamic regulatory interface housing specialized proteins-including voltage-dependent anion channels (VDACs) [7], translocase complexes (TOM/TIM) [8], and the redox-sensitive protein mitoNEET (CISD1)-that coordinate metabolite exchange, energy signaling, and mitochondrial quality control. MitoNEET is a small [2Fe-2S] cluster-binding protein anchored to the OMM by a single transmembrane helix, with its functional domain exposed to the cytosol, present at approximately 1,000-5,000 dimers per mitochondrion [4,5,9]. It belongs to the NEET protein family alongside NAF-1 (CISD2), both defined by a unique CDGSH [2Fe-2S]-binding motif [10,11] and operating at mitochondria-associated membrane (MAM) contact sites to coordinate iron homeostasis, ROS signaling, and cell survival decisions between the OMM and endoplasmic reticulum. Functionally, mitoNEET acts as a metabolic gatekeeper: coordinating Fe-S cluster transfer

to inner-membrane respiratory complexes and stabilizing early electron flow to support high-efficiency oxidative phosphorylation [4,12]. Impairment-through structural damage, Fe-S transfer loss, or pathological downregulation-drives a shift toward glycolysis

(approximately two ATP/glucose versus approximately 36 via OXPHOS), promoting ROS accumulation and lactate buildup across conditions including insulin resistance, neurodegeneration, cardiovascular disease, and cancer.

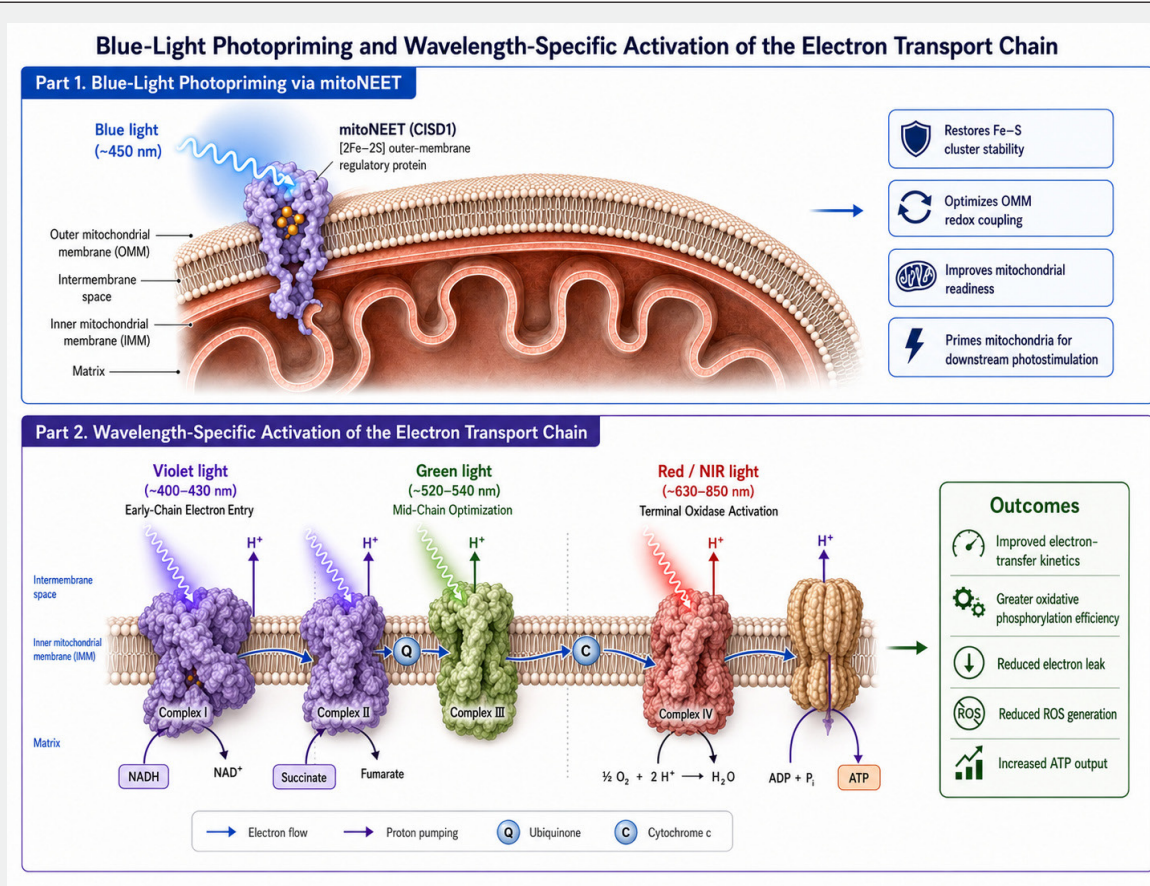


Figure 1: Proposed Model of Blue-Light Photopriming via mitoNEET and Sequential Wavelength-Specific Modulation of the Electron Transport Chain.

Mitochondria are highly dynamic organelles that continuously undergo fusion, fission, and biogenesis to maintain metabolic efficiency and adapt to changing energy demands, with the OMM playing a central coordinating role in each process. During fusion, the GTPase proteins Mitofusin 1 (MFN1) and Mitofusin 2 (MFN2) [13,14], embedded in the OMM, act as tethering factors that physically link adjacent mitochondria, enabling the exchange of lipids, mitochondrial DNA, and metabolic components to dilute damaged constituents and preserve bioenergetic balance. During fission, the OMM provides the structural platform for recruitment of Dynamin-related protein 1 (DRP1) [15], a cytosolic GTPase that assembles at constriction sites to sever the membrane, enabling segregation of damaged regions, metabolic remodeling under stress, and equal mitochondrial distribution during cell division. Mitochondrial biogenesis additionally depends on OMM-mediated cross-talk with the endoplasmic reticulum to exchange the lipids and calcium required for new membrane formation.

Because mitoNEET simultaneously governs Fe-S cluster transfer, outer-membrane redox coupling, ROS modulation, and metabolic fuel switching, its dysfunction converges across a broad spectrum of chronic disease. In neurodegenerative conditions (Parkinson’s disease, Alzheimer’s disease, ALS), impaired mitoNEET redox control disrupts the fine ATP/ROS balance required by metabolically demanding neurons [16]. In cancer, tumor cells upregulate mitoNEET to exploit its ROS-buffering capacity and support Warburg-type metabolic flexibility [11]. In type 2 diabetes and insulin resistance, mitoNEET links OMM redox status directly to ROS-mediated insulin signaling and fuel selection [12]. In chronic inflammatory and autoimmune conditions-including rheumatoid arthritis and chronic pain-downstream ROS amplifies inflammatory cascades, while in aging and fatigue-related syndromes, progressive decline in mitoNEET expression reduces mitochondrial redox adaptability and systemic energy resilience [17].

Mitophagy is the selective autophagic removal of damaged or superfluous mitochondria and serves as one of the cell's most important quality-control mechanisms, preventing the persistence of mitochondria that have lost membrane potential, accumulated excess iron, generated excessive ROS, or become inefficient at oxidative phosphorylation. By removing defective mitochondria, mitophagy preserves ATP-generating capacity, maintains redox balance, restrains inflammatory signaling, and protects metabolically demanding tissues such as brain, heart, and skeletal muscle from progressive bioenergetic decline. Impairment of mitophagy has been linked to aging, neurodegeneration, cardiometabolic dysfunction, and chronic inflammatory disease [18,19]. Within this framework, C1SD1 has been identified as a Parkin substrate, directly linking mitoNEET to the PINK1/Parkin mitophagy pathway [18-20]. Because Parkin-mediated ubiquitination of OMM proteins is a core step in stress-induced mitophagy, inclusion of C1SD1 in this substrate network places mitoNEET at the interface between mitochondrial performance and mitochondrial turnover.

Emerging data further suggest that mitoNEET is not merely a

passive participant in mitophagy signaling, but an active modulator of whether mitophagy proceeds efficiently. Pharmacologic inhibition of mitoNEET promotes accumulation of PINK1 and Parkin and induces PINK1/Parkin-mediated mitophagy [21], indicating that mitoNEET can act as a restraint on mitochondrial clearance under certain conditions. Consistent with this view, accumulation of C1SD proteins during aging and in Pink1/Parkin-deficient models blocks mitophagy and contributes to pathology [21], supporting the concept that appropriate regulation and turnover of C1SD1 are required for normal mitochondrial quality control. This dual role is biologically important: under basal conditions, mitoNEET supports mitochondrial efficiency by coordinating Fe-S cluster biology, redox buffering, and oxidative metabolism, while under stress it influences the threshold between mitochondrial preservation and disposal. These findings establish mitoNEET not as simply pro- or anti-mitophagy, but as a redox-sensitive outer-membrane regulator that tunes quality-control responses according to the metabolic state of the cell, with implications for durable photobiomodulatory effects on the mitochondrial network (Figure 2).

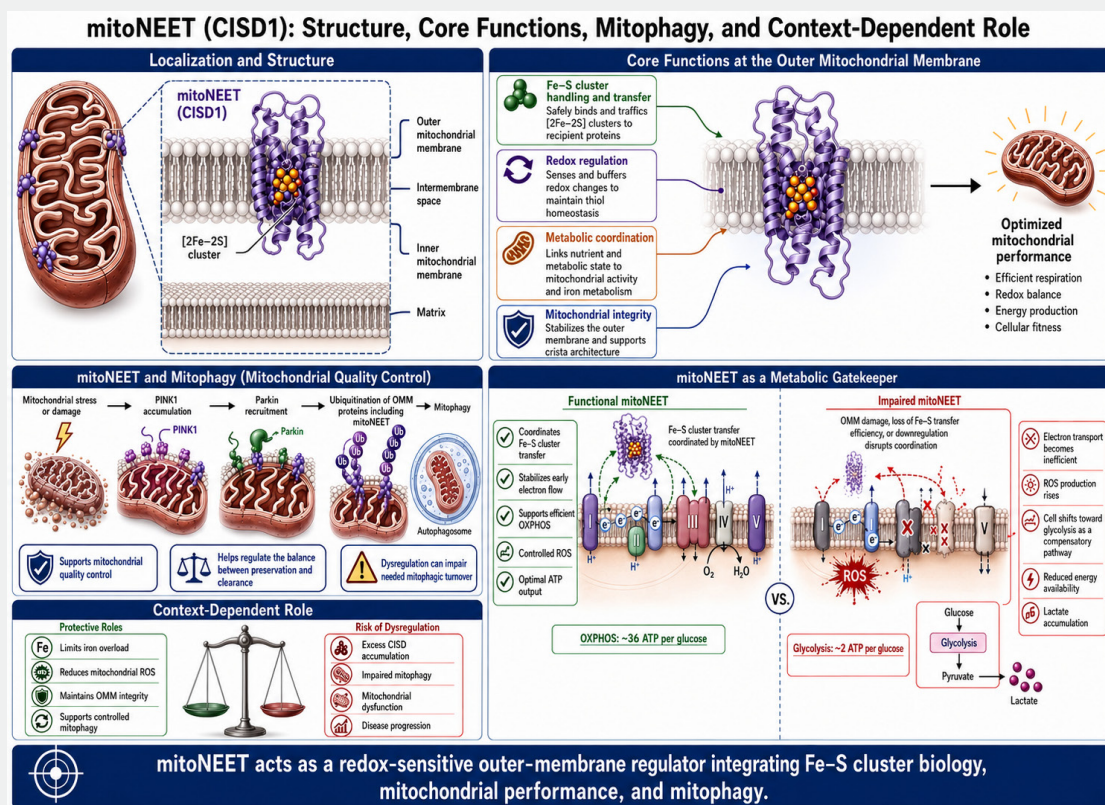


Figure 2: MitoNEET/C1SD1 as a Redox-Sensitive Outer Mitochondrial Membrane Regulator of Mitochondrial Function, Mitophagy, and Metabolic Balance.

Blue laser photoprimering: concept and mechanistic framework

The concept of photoprimering introduces an initial blue-laser exposure applied to the target tissue before full LLLT treatment. Blue wavelengths preferentially interact with components of the outer cellular and mitochondrial membranes-most notably the [2Fe-2S]-containing regulatory protein mitoNEET, which exhibits strong absorption in this spectral range [4,5]. Photostimulation at this stage helps restore Fe-S cluster stability, optimize redox coupling across the outer membrane, and re-establish conditions favorable for efficient downstream electron handling. In this way, blue-light priming functionally prepares the mitochondrial network for more robust metabolic activation. Following the priming step, subsequent irradiation with violet, green, or red/NIR wavelengths engages their respective inner-membrane targets-including ETC Complexes I through IV-to drive electron transport and oxidative phosphorylation. This two-stage sequence, outer-membrane photoprimering followed by inner-membrane photostimulation, represents a mechanistic hierarchy in LLLT in which the readiness of the OMM determines

the magnitude of the bioenergetic response to inner-membrane photons. The net result is improved electron-transfer kinetics, greater oxidative phosphorylation efficiency, reduced electron leak and ROS generation, and ultimately increased cellular ATP output.

Molecular Evidence: CISD1 expression analysis

Participants with low-to-normal baseline expression

An experimental biochemical evaluation was conducted by Marisol Peña-Sánchez, MSc (Science), MSc (Neurosciences), MSc (Biochemistry), PhD, Full Assistant Professor in the Neurobiology Laboratory at the Rafael Estrada González Institute, to quantify alterations in CISD1 (mitoNEET) expression following two weeks of blue-laser photostimulation (450 nm, 5 min per session, three sessions per week). Using five independent analytical platforms-Western blot, ELISA, mass spectrometry, immunoprecipitation coupled to Western blot, and immunofluorescence-the investigation assessed pre-treatment versus Day 14 CISD1 levels in five human participants.

Table 1: CISD1 percent change from baseline to Day 14 in participants with low-to-normal baseline CISD1 expression following blue laser photostimulation (450 nm, 5 min/session, 3x/week). Positive values indicate post-treatment upregulation. Abbreviations: WB, Western blot; ELISA, enzyme-linked immunosorbent assay; MS, mass spectrometry; IF/IHC, immunofluorescence/immunohistochemistry; IP+WB, immunoprecipitation-coupled Western blot.

Participant	WB (%)	ELISA (%)	MS (%)	IF/IHC (%)	IP+WB (%)
P-01	+8.85	+6.15	+4.75	+5.24	+2.48
P-02	+1.87	+6.47	+9.14	+5.26	+8.76
P-03	+25.11	+26.06	+19.62	+23.78	+21.29
P-04	+23.57	+20.56	+27.50	+27.80	+19.93
P-05	+25.72	+29.39	+21.52	+27.92	+29.95

Across all analytical platforms, CISD1 displayed a uniform post-treatment increase following blue-light exposure in participants with low-to-normal baseline CISD1 levels. The data also reveal clear inter-individual variability: three participants demonstrated moderate CISD1 elevations in the 20-30% range, whereas two participants showed more modest increases of approximately 6%. This heterogeneity aligns with the variability reported in other investigations of mitochondrial protein regulation and suggests that baseline redox balance, Fe-S cluster turnover, or iron-handling capacity may influence the degree of photonic responsiveness. Notably, no analytical method showed a reduction in CISD1 expression for any participant in this cohort, and no assay produced an opposing directional effect. This cross-platform concordance supports the interpretation that short-term blue-laser exposure reliably enhances CISD1 abundance at the mitochondrial outer membrane in participants with low-to-normal baseline expression (Table 1).

Participants with elevated baseline expression

A complementary investigation examined CISD1 responses to the identical blue-laser protocol in five participants with elevated baseline CISD1 levels: two with metabolic syndrome (P-SM01, P-SM02), one with type 2 diabetes mellitus of 11 years' duration (P-DM11), and two with oncological diagnoses (P-CC06, colon cancer; P-CM03, breast cancer). Baseline CISD1 values in this cohort exceeded the threshold of elevated expression across all five assay platforms (Western blot ≥ 1.20 , ELISA ≥ 0.80 ng/mL, mass spectrometry $\geq 13,500$ arbitrary intensity units, immunoprecipitation + Western blot ≥ 1.28 , and immunofluorescence ≥ 29.0 mean intensity). Blood samples were collected at baseline (Day 0) and following six blue-laser sessions administered over 14 days (three sessions per week, 5 minutes per session at 450 nm). In striking contrast to the upregulation observed in participants with low-to-normal baseline CISD1, participants in this elevated-baseline cohort demonstrated a

mild but consistent downward modulation following blue-laser exposure. The metabolic and diabetic participants (P-SM01, P-SM02, P-DM11) showed small but consistent reductions across all five assay platforms, ranging from approximately -4% to -8% depending on the assay and individual. Specifically, Western blot reductions ranged from -5.02% to -6.04%; ELISA reductions from -5.03% to -7.02%; mass spectrometry reductions from -3.89% to -5.19%; immunoprecipitation + Western blot reductions from -4.92% to -6.52%; and immunofluorescence reductions from -3.93% to -6.14%. The two oncological participants (P-CC06, P-CM03) exhibited near-stable CISD1 levels across all platforms, with changes of only -0.18% to -1.80%, consistent with a relatively stable protein expression profile under the current protocol.

Cross-platform directional consistency was preserved in Western blot, ELISA, mass spectrometry, immunoprecipitation + Western blot, and immunofluorescence for all participants, supporting the internal validity of the observed biomodulation signal. Taken together, the findings from both cohorts-low-to-normal baseline (upregulation, +6% to +30%) and elevated baseline (mild downregulation, -4% to -8% in metabolic/diabetic participants; near-stable in oncological participants)-demonstrate a bidirectional, baseline-dependent biomodulation

of CISD1 by visible blue laser at 450 nm. This pattern is consistent with the established concept of LLLT hormesis, wherein the biological response to photonic stimulation is governed by the pre-existing physiological state of the target tissue. When CISD1 is deficient or suppressed, blue-laser exposure drives upregulation, restoring outer mitochondrial membrane regulatory capacity and improving the conditions for efficient electron transport chain activity. Conversely, when CISD1 is already elevated above physiological norms-as may occur in compensatory metabolic stress responses-blue-laser exposure produces a mild normalizing reduction, suggesting a homeostatic regulatory mechanism rather than simple linear stimulation. This bidirectional responsiveness distinguishes CISD1 modulation by blue laser from a simple excitatory photochemical event and positions it as a true biomodulatory interaction: one that moves protein expression toward an optimized functional range regardless of starting point. The magnitude, directionality, and cross-platform consistency of this effect across both cohorts provide internally consistent multi-assay evidence that short-term blue-laser photoprimering reliably modulates CISD1 at the mitochondrial outer membrane in a physiologically adaptive manner. Table 2 summarizes the elevated-baseline cohort percent-change results across analytical platforms (Table 2).

Table 2: CISD1 percent change from baseline to Day 14 in participants with elevated baseline CISD1 expression. Metabolic syndrome and type 2 diabetes participants exhibited mild downward modulation (-4% to -8%); oncological participants demonstrated near-stable expression (-0.2% to -1.8%). Abbreviations: WB, Western blot; ELISA, enzyme-linked immunosorbent assay; MS, mass spectrometry; IF/IHC, immunofluorescence/immunohistochemistry; IP+WB, immunoprecipitation-coupled Western blot.

Patient	Condition	WB (%)	ELISA (%)	MS (%)	IF/IHC (%)	IP+WB (%)
P-SM01	Metabolic Syndrome	-5.29	-5.03	-3.89	-3.93	-5.19
P-SM02	Metabolic Syndrome	-5.02	-5.41	-4.34	-4.60	-4.92
P-DM11	Type 2 Diabetes (11 yr)	-6.04	-7.02	-5.19	-6.14	-6.52
P-CC06	Colon Cancer (6 yr)	-0.73	-0.48	-0.20	-0.67	-1.42
P-CM03	Breast Cancer (3 yr)	-0.49	-0.49	-0.18	-0.66	-0.75

Biochemical Evidence: blue laser photoprimering plus red versus red-only LLLT

A randomized crossover experiment conducted by Dr. Calixto Machado, MD, PhD, FAAN (Full Professor, Institute of Neurology and Neurosurgery, Havana), evaluated acute biochemical responses in ten adults following two LLLT protocols: (1) red-only laser therapy (13 minutes at 635 nm) and (2) blue laser therapy (5 minutes at 450 nm) followed by red laser therapy (13 minutes at 635 nm). Venous blood samples were obtained immediately prior to the intervention and again 10 minutes following treatment. Biomarkers included plasma and red-blood-cell (RBC) thiobarbituric-acid-reactive substances (TBARS), superoxide dismutase (SOD), catalase (CAT), glutathione (GSH), and plasma lactate/pyruvate (L/P) ratio. Outcomes demonstrated both LLLT conditions produced statistically significant within-subject biochemical shifts consistent with rapid improvement

in redox balance. The addition of a blue-laser photoprimering phase markedly potentiated the antioxidant and redox-balancing effects of subsequent red low-level laser therapy (LLLT), with the most pronounced differences observed in erythrocyte-based biomarkers. The larger rise in RBC glutathione (GSH) and the partial preservation of catalase (CAT) activity under the blue/red condition suggest enhanced regeneration of reduced glutathione and reduced reliance on enzymatic peroxide detoxification. Together, these effects indicate a shift toward a more reduced intracellular redox environment, improved buffering against reactive oxygen species (ROS), and more stable redox cycling within erythrocytes.

Blue photoprimering also reversed the suppression of superoxide dismutase (SOD) observed in the red-only condition. This reversal implies restoration of superoxide-clearing capacity early in the LLLT response. Because SOD serves as the first enzymatic

line of defense against mitochondrial-derived superoxide, this finding suggests that blue-wavelength stimulation stabilizes Fe-S-dependent antioxidant systems. This interpretation is further supported by the increase in CISD1 (mitoNEET) expression observed in the parallel molecular study. CISD1 is a key regulator of outer mitochondrial membrane iron-sulfur cluster transfer and redox coupling; its upregulation may improve electron flux into the respiratory chain and support more efficient detoxification of ROS generated during periods of elevated mitochondrial metabolism. Although both LLLT protocols enhanced oxidative metabolism-as reflected by similar reductions in the lactate/pyruvate (L/P) ratio-the blue-primed red treatment achieved a more favorable balance between antioxidant enzyme activity and metabolic oxidation. This balance is consistent with more efficient

electron transport chain (ETC) coupling, reduced electron leak, and lower oxidative strain per unit of metabolic activity.

The rapid emergence of these biochemical changes-occurring within ≤ 10 minutes post-irradiation-demonstrates that blue photoprimering produces an additive and synergistic effect on systemic redox biomarkers, rather than simply functioning as an additional energy dose. The magnitude of benefit is biologically meaningful: approximately a 180% greater increase in RBC GSH and a 57% greater recovery of RBC SOD under blue-primed conditions compared to red-only LLLT. Such changes are consistent with early mitochondrial signaling events that precede ATP upregulation, including adjustments in ROS setpoints, membrane potential stabilization, and redox-sensitive protein activation. (Table 3&4)

Table 3: Pre- and post-treatment plasma and erythrocyte biomarker changes: red laser-only group (n = 10). Values represent group means. CAT, catalase; GSH, glutathione; L/P, lactate/pyruvate ratio; TBARS, thiobarbituric acid-reactive substances; SOD, superoxide dismutase. Statistically significant changes ($p < 0.05$) are highlighted.

Biomarker	Mean Pre	Mean Post	Mean Delta	SEM	T-test p	Wilcoxon p
Plasma TBARS (nM)	1942.54	1634.71	-307.83	73.32	0.002	0.014
Plasma SOD (U/mL)	14.74	11.74	-3.00	0.86	0.007	0.027
Plasma CAT (U/L)	236.03	219.28	-16.75	6.28	0.026	0.037
Plasma GSH (ug/mL)	372.70	269.20	-103.50	25.31	0.003	0.002
RBC TBARS (nM)	45.87	135.50	+89.63	28.27	0.011	0.027
RBC SOD (U/mL)	9.03	5.45	-3.58	1.54	0.045	0.020
RBC CAT (U/L)	252.89	213.71	-39.18	6.28	<0.001	0.004
RBC GSH (ug/mL)	310.76	337.30	+26.54	34.29	0.459	0.557
Plasma L/P Ratio	16.61	10.03	-6.58	1.08	<0.001	0.004

Table 4: Pre- and post-treatment plasma and erythrocyte biomarker changes: blue laser photoprimering followed by red laser group (n = 10).

Biomarker	Mean Pre	Mean Post	Mean Delta	SEM	T-test p	Wilcoxon p
Plasma TBARS (nM)	1933.72	1612.79	-320.93	71.57	0.002	0.004
Plasma SOD (U/mL)	14.77	10.62	-4.15	0.88	0.001	0.002
Plasma CAT (U/L)	231.76	211.05	-20.71	3.78	<0.001	0.002
Plasma GSH (ug/mL)	383.10	282.90	-100.20	25.80	0.004	0.002
RBC TBARS (nM)	44.30	71.21	+26.91	9.06	0.016	0.014
RBC SOD (U/mL)	8.91	10.48	+1.57	0.59	0.026	0.027
RBC CAT (U/L)	253.14	237.43	-15.71	5.19	0.014	0.037
RBC GSH (ug/mL)	293.63	369.16	+75.53	31.54	0.040	0.049
Plasma L/P Ratio	14.50	8.47	-6.04	0.82	<0.001	0.004

Taken together, these results provide quantitative biochemical evidence supporting the mechanistic model in which outer-mitochondrial-membrane photoprimering using blue wavelengths enhances the efficiency, redox balance, and metabolic responsiveness of mitochondria during subsequent red-light LLLT. The convergence of erythrocyte antioxidant markers, L/P ratio shifts, and molecular CISD1 upregulation underscores a coherent physiological response that integrates membrane-level

photochemistry with systemic metabolic regulation. Building on this mechanistic and biochemical evidence, the present prospective clinical study evaluated whether sequential blue 450 nm laser photoprimering followed by standard red 635 nm laser therapy is non-inferior-and potentially superior-to standard red laser therapy alone in providing temporary relief of nociceptive musculoskeletal pain.

Materials and Methods

Study design

A prospective, multi-site, single-arm non-inferiority clinical study (ClinicalTrials.gov identifier: NCT07121933; IRB: WCG IRB, WIRB Tracking No. 20253018, Puyallup, WA) was conducted to evaluate whether sequential blue 450 nm laser photoprimering (Erchonia PR1ME450) followed by standard red laser 635 nm therapy (Erchonia Corp.) is non-inferior to i.e., equivalent to or superior to standard red laser therapy alone (Erchonia Corp.) in providing temporary relief of nociceptive musculoskeletal pain. Three geographically distributed investigational sites enrolled subjects: Wautier Wellness Chiropractic (Marquette, MI; PI: Stephanie Wautier, DC, RN), New York ChiroCare (White Plains, NY; PI: Robert Silverman, DC, DACBN), and Gair Laser Chiropractic (West Covina, CA; PI: Kirk Gair, DC).

Participants

Eligible subjects were adults aged 22 years or older presenting with chronic (≥30 consecutive days) neck and/or shoulder pain of musculoskeletal origin diagnosed as osteoarthritis (degenerative joint disorder), chronic muscle spasms, or cervical and thoracic spine sprain/strain, with a baseline self-reported pain intensity of ≥50 on the 0-100 Visual Analog Scale (VAS). Key exclusion criteria included acute pain, active chronic pain disease (e.g., fibromyalgia), use of analgesics or muscle relaxants within 7 days prior to treatment, prior neck/shoulder surgery, herniated disc, active cancer or cancer treatment within 6 months, and unstable cardiac disease.

Treatment protocol

Each enrolled subject received a single sequential treatment session consisting of 5 minutes of blue laser photoprimering (450 nm, 8.75 mW per diode, bidirectional sweeping across the bilateral neck and shoulder region at 2-3 inches from skin surface) followed immediately by 13 minutes of standard red laser therapy (635 nm, per the same protocol used in the 2001 historical reference trial, K012580), for a total treatment duration of 18 minutes. The historical reference dataset used for non-inferiority comparison consisted of the active treatment group (n = 43) from the 2001

clinical trial whose results supported 510(k) clearance K012580 for red laser therapy alone.

Outcome measures

The primary efficacy outcome measure was the change in subject self-reported VAS pain rating from baseline to study endpoint (within 3 minutes of treatment completion). Individual subject success was defined as a ≥30% decrease in VAS score from baseline to endpoint. Overall study success was predefined as ≥65% ± 5% of subjects meeting the individual success criterion, yielding a non-inferiority threshold of ≥60% responders. Secondary outcome measures included VAS pain ratings at 24 and 48 hours post-treatment, neck and shoulder range of motion (ROM) by inclinometry, subject satisfaction ratings (5-point Likert scale), and adverse event surveillance.

Statistical analysis

Statistical analyses included a two-sample independent proportions test for responder rate comparison, a correlated-samples Student’s t-test for within-group VAS change, an independent-samples t-test for between-group VAS change comparison, and 95% confidence interval (CI) calculation for the between-group responder rate difference. Statistical analysis was conducted by an independent statistical consultant, Elvira Cawthon.

Subject characteristics and baseline variables

Forty-four (44) subjects were enrolled and all 44 completed the study through endpoint assessment; the intent-to-treat and per-protocol populations were therefore identical, and no missing data imputation was required for primary efficacy analysis. For post-treatment follow-up evaluations, one subject was lost, yielding n = 43 for secondary time-point analyses. The subject sample was 55% male (n = 24) and 45% female (n = 20), predominantly Caucasian (64%) and Hispanic (23%), with a mean age of 54.18 ± 13.51 years (range 23-85). No statistically significant difference in age by gender was observed (p = 0.637). Table 5 summarizes subject demographics and key baseline pain variables (Table 5).

Table 5: Subject demographics and baseline pain characteristics for the blue + red treatment group (n = 44).

Characteristic	Value (n = 44)
Male / Female	55% / 45%
Mean age, years (SD; range)	54.18 (13.51; 23-85)
Ethnicity (Caucasian / Hispanic / other)	64% / 23% / 13%
Baseline VAS, mean (SD)	74.50 (9.91)
Mean pain duration, months (SD; median)	91.30 (108.75; 49)
Subjects using analgesic or pain medication at baseline	50% (n = 22)
Subjects using non-drug pain therapies at baseline	64% (n = 28); chiropractic 48%

Subjects in the current study presented with meaningfully higher baseline pain severity (mean VAS 74.50 vs. 60.21) and longer pain chronicity (mean 91.30 vs. 61.74 months; median 49 vs. 38 months), though the duration difference did not reach statistical significance. Among the 50% of current-study subjects using pharmacological pain management at baseline, ibuprofen (31%) and acetaminophen/Tylenol (19%) were most

commonly reported; 69% used medication on an as-needed basis. Chiropractic care was the predominant non-pharmacological therapy (48%), followed by physical therapy (16%) and massage (14%), with 40% of non-drug therapy users engaging in treatment only as needed. Concomitant medications for non-pain indications were reported by 39% of subjects (n = 17), most commonly antihypertensives (8 subjects).

Result

Primary efficacy: Responder Rate

Table 6: Primary efficacy outcome: responder rate ($\geq 30\%$ VAS reduction) and VAS change scores from baseline to endpoint for the blue + red group and the 2001 historical red-only reference group. * $p < 0.0001$ within-group (correlated-samples t-test). Between-group responder rate difference: $p = 0.042$ (two-sample independent proportions test). Between-group VAS change: $p = 0.061$ (independent-samples t-test, not significant). Abbreviations: CI, confidence interval; SD, standard deviation; VAS, Visual Analog Scale.

Efficacy Measure	Blue + Red (n = 44)	Red Only (n = 43)
Responder rate ($\geq 30\%$ VAS reduction)	84.09%	65.10%
Between-group difference (95% CI); p-value	+18.97% (1.09, 36.86); $p = 0.042$	-
Baseline VAS, mean (SD)	74.50 (9.91)	60.21 (9.84)
Endpoint VAS, mean (SD)	33.59 (20.91)	31.19 (18.74)
Mean VAS change, baseline to endpoint (SD)	-37.50 (20.93)*	-29.02 (20.71)

The study met and exceeded its prespecified non-inferiority success criterion, demonstrating a statistically higher responder rate for the blue + red sequential protocol compared with red laser therapy alone. Eighty-four point one percent (84.09%) of subjects treated with blue + red achieved the individual success criterion ($\geq 30\%$ VAS reduction) compared with 65.10% of subjects in the 2001 reference group treated with the red laser diode alone—a between-group difference of +18.97% in favor of the blue-primed sequential protocol, which was statistically significant ($z = 2.036$, $p = 0.042$). The 84.09% responder rate exceeded not only the lower non-inferiority boundary of 60% (by 24.09 pp) but also the upper equivalence boundary of 70% (by 14.09 pp), supporting a treatment effect beyond non-inferiority in this historical-control comparison. The 95% CI for the between-group difference in responder rates was (1.09, 36.86); as the entire interval lies above zero, the finding supports a treatment effect favoring the blue-primed sequential protocol. Table 6 presents primary efficacy data and VAS change scores (Table 6).

VAS pain scores

Within the blue + red group, the mean VAS score decreased by 37.50 points from baseline (74.50) to endpoint (33.59), representing a clinically meaningful transition from the upper-moderate-to-severe pain range to mild pain in a single treatment session ($p < 0.0001$). Despite starting from a meaningfully higher baseline (74.50 vs. 60.21, $p < 0.0001$), subjects receiving blue photoprimer achieved comparable absolute endpoint pain levels to those receiving red laser therapy alone (33.59 vs. 31.19), with a superior responder rate, consistent with a genuine enhancement

effect of the blue pretreatment.

VAS pain ratings were assessed at four time points (baseline, endpoint, 24 h, and 48 h post-treatment). In the blue + red group (n = 43 for follow-up), mean VAS scores continued to decline progressively through the post-treatment period: 74.50 (baseline) \rightarrow 33.59 (endpoint) \rightarrow 24.93 (24 h) \rightarrow 21.09 (48 h) (see Figure 3). By contrast, the red-only group (n = 34 for follow-up) demonstrated a reduction from baseline (60.21) to endpoint (31.19) that then plateaued across the 48-hour follow-up period (34.03 at 24 h; 34.18 at 48 h). This progressive, sustained reduction in the blue + red group—in contrast to the plateau observed with red laser alone—suggests that blue photoprimer confers a durable preconditioning effect that supports continued bioenergetic recovery beyond the immediate treatment period (Figure 3).

Range of motion

Range of motion (ROM) improved substantially following the single treatment session across all measured planes. Mean shoulder ROM in seated passive abduction improved by +24.16° on the right and +19.25° on the left; shoulder ROM in the relaxed position improved by +22.34° on the right and +22.00° on the left. Neck ROM improved by +14.77° on the right and +14.48° on the left. In each case, post-treatment ROM approached or reached the clinically normal range (170-180° for shoulder; 70-90° for neck), representing a meaningful functional restoration from the depressed pre-treatment values. ROM data were not available for the 2001 historical reference group and therefore cannot be directly compared.

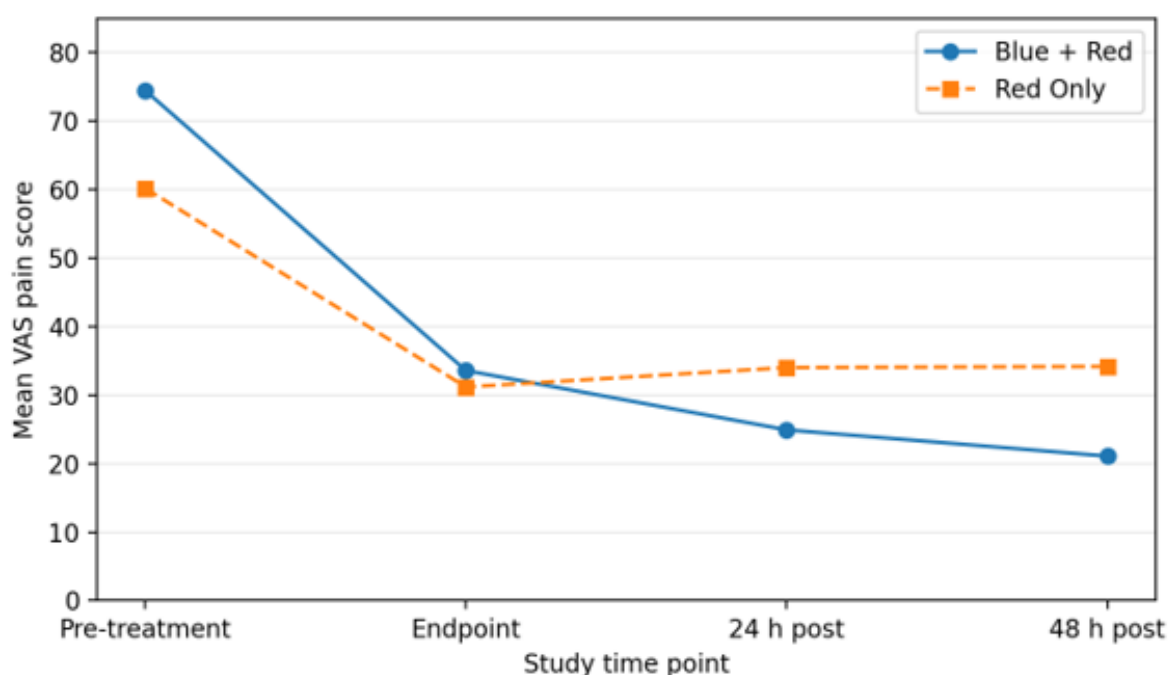


Figure 3: Mean neck and shoulder pain VAS ratings across study duration: blue + red versus red only.

Subject satisfaction and safety

Subject satisfaction with treatment outcome was high at all time points. At endpoint, 91% of subjects ($n = 44$) rated themselves as “Very Satisfied” (68%) or “Somewhat Satisfied” (23%). Satisfaction remained elevated at 86% at 24 hours and 88% at 48 hours, markedly exceeding the “positive outcome satisfaction” threshold of 50% established in prior Erchonia clinical trials. No adverse events were recorded or reported by any subject or investigator at any test site throughout the duration of the study, including the 48-hour post-treatment follow-up period, consistent with the established safety profile.

Discussion

The findings support a mechanistic framework in which wavelength-specific activation may be initiated at the mitochondrial outer membrane, suggesting that blue-laser photoprimering can enhance subsequent oxidative phosphorylation. The significance of these findings lies in the integration of molecular, biochemical, and clinical evidence. Clinically, a prospective multi-site controlled study (NCT07121933; $n = 44$) demonstrated that a single session of sequential blue laser photoprimering (450 nm, five minutes) followed by standard red laser therapy (635 nm, 13 minutes) produced a statistically higher responder rate compared with historical red-laser-only controls (84.09% vs. 65.10%), with progressive VAS pain reductions continuing through 48

hours post-treatment and clinically meaningful improvements in cervical and shoulder range of motion approaching normal reference values in a single treatment session. The molecular data confirmed that blue laser exposure regulates C1SD1 expression in a bidirectional, baseline-dependent manner: producing upregulation of approximately 6-30% in participants with low-to-normal baseline expression and mild attenuation of 4-8% in participants with metabolically elevated baseline C1SD1 levels, suggesting activation of redox-regulatory proteins in the outer mitochondrial membrane. The biochemical evidence further demonstrated that pre-exposure to blue light amplified red-laser effects on antioxidant systems, producing greater increases in GSH and SOD and reducing CAT consumption.

Together, these outcomes indicate that blue laser photoprimering restores redox equilibrium, supports iron-sulfur cluster transfer, and enhances electron flux through the ETC. Furihata et al. (2021) showed that loss of mitoNEET expression in cardiac tissue led to impaired mitochondrial morphology, elevated ROS, and decreased respiratory capacity [17]. The observed increase in C1SD1 expression following blue-laser exposure therefore likely reflects a biologically meaningful enhancement in mitochondrial redox control and Fe-S cluster integrity. Because C1SD1's [2Fe-2S] cofactor plays a central role in electron transfer and iron homeostasis at the outer membrane, its upregulation suggests improved capacity for maintaining redox balance and supporting

downstream oxidative phosphorylation. Upregulation of this protein may facilitate more efficient trafficking of Fe-S clusters to inner-membrane complexes (I-III), improving downstream oxidative phosphorylation. Enhanced CISD1 activity also supports tighter redox control, reducing ROS accumulation and improving mitochondrial membrane potential ($\Delta\Psi_m$). These molecular outcomes align with prior studies indicating that improved CISD1 function enhances mitochondrial efficiency and antioxidant capacity.

When mitoNEET is dysfunctional or oxidatively damaged, the ETC cannot efficiently receive or utilize redox substrates, leading to metabolic inefficiency and reduced ATP output—even when traditional LLLT wavelengths are applied, including violet, green, and red/NIR light. Although these wavelengths directly stimulate inner-membrane respiratory complexes, their biological effectiveness ultimately depends on the functional integrity of the mitochondrial outer membrane, which serves as the initial regulatory interface for energy metabolism. Thus, the readiness of the outer membrane—and specifically mitoNEET's capacity to support Fe-S cluster transfer and maintain redox balance—determines how effectively downstream photobiological interactions can drive oxidative phosphorylation. In this way, blue laser photopriming represents not merely an additive wavelength, but the initiation of a new sequential model of mitochondrial modulation: outer-membrane priming followed by inner-membrane activation. Future investigations should continue to examine how mitochondrial membrane cross-talk, Fe-S cluster dynamics, and sequential wavelength exposure can be optimized to improve clinical outcomes across pain management, metabolic health, and neurodegenerative applications.

Conclusion

Blue-laser photopriming introduces a new mechanistic paradigm in LLLT by supporting a model in which photonic activation may be initiated at the mitochondrial outer membrane through mitoNEET-dependent redox restoration. This priming effect enhances the downstream bioenergetic responses to traditional LLLT wavelengths that act directly on the inner mitochondrial ETC, yielding more efficient oxidative phosphorylation. At the molecular level, blue-laser exposure produced bidirectional, baseline-dependent regulation of CISD1 (mitoNEET) across all five independent analytical platforms, confirming a true biomodulatory rather than simply excitatory effect. Biochemically, blue photopriming amplified the redox-balancing effects of subsequent red laser therapy, producing substantially greater increases in erythrocyte glutathione and superoxide dismutase activity relative to red-only LLLT. Clinically, a prospective multi-site controlled study demonstrated a statistically higher responder rate for the sequential blue-then-red protocol compared with historical red-laser-only controls, with progressive pain reduction sustained through 48 hours following a single treatment session. The convergence of these

molecular, biochemical, and clinical findings supports a unified biological model that meaningfully advances the field of low-level laser therapy and establishes blue laser photopriming as a clinically relevant upstream intervention to optimize outcomes.

Additional Information

Ethics approval and consent to participate

The clinical study was reviewed and approved by WCG IRB, WIRB Tracking No. 20253018. Written informed consent was obtained from all participants prior to enrollment. The study was registered at ClinicalTrials.gov under identifier NCT07121933.

Conflict of interest

T.S. and S.S. are employees of Erchonia Corporation, the manufacturer of the Erchonia PR1ME450 and XLR8 laser devices evaluated in this manuscript and the sponsor of the clinical study. R.S., K.G., and S.W. conducted the clinical study at independent test sites and declare no competing interests.

Funding

Erchonia Corporation funded the clinical study, provided the investigational devices, supplied device-use training to the investigational sites, and retained an independent statistical consultant, Elvira Cawthon, to assist with statistical analysis.

Author contributions

Concept and design: T.S., S.S. Acquisition, analysis, or interpretation of data: T.S., S.S., R.S., K.G., S.W. Drafting of the manuscript: T.S., S.S. Critical revision of the manuscript for important intellectual content: T.S., S.S., R.S., K.G., S.W. Administrative, technical, or material support: R.S., K.G., S.W. Supervision: T.S., S.S.

Acknowledgment

The authors wish to acknowledge Marisol Peña-Sánchez, MSc, PhD, Neurobiology Laboratory, Rafael Estrada González Institute, for conducting the molecular CISD1 investigations described in this manuscript, and Calixto Machado, MD, PhD, Institute of Neurology and Neurosurgery, Havana, Cuba, for conducting the biochemical oxidative stress study described in this manuscript. Both investigators provided independent laboratory data that contributed substantially to the findings of this article.

Data availability

The clinical study was registered on ClinicalTrials.gov under identifier NCT07121933. Additional study data are available from the corresponding author upon reasonable request, subject to applicable privacy, ethical, and regulatory restrictions.

References

1. Hamblin MR (2017) Mechanisms and applications of the anti-inflammatory effects of photobiomodulation. *AIMS Biophys* 4(3): 337-361.

- Karu TI (2008) Mitochondrial signaling in mammalian cells activated by red and near-IR radiation. *Photochem Photobiol* 84(5): 1091-1099.
- De Freitas LF, Hamblin MR (2016) Proposed mechanisms of photobiomodulation or low-level light therapy. *IEEE J Sel Top Quantum Electron* 22(3): 7000417.
- Wiley SE, Murphy AN, Ross SA, Van Der Geer P, Dixon JE (2007) MitoNEET is an iron-containing outer mitochondrial membrane protein that regulates oxidative capacity. *Proc Natl Acad Sci USA* 104(13): 5318-5323.
- Paddock ML, Wiley SE, Axelrod HL, Cohen AE, Roy M, et al. (2007) MitoNEET is a uniquely folded 2Fe-2S outer mitochondrial membrane protein stabilized by pioglitazone. *Proc Natl Acad Sci USA* 104(36): 14342-14347.
- Chung H, Dai T, Sharma SK, Huang YY, Carroll JD, et al. (2012) The nuts and bolts of low-level laser (light) therapy. *Ann Biomed Eng* 40(2): 516-533.
- Colombini M (2012) VDAC structure, selectivity, and dynamics. *Biochim Biophys Acta* 1818(6): 1457-1465.
- Wiedemann N, Frazier AE, Pfanner N (2004) The protein import machinery of mitochondria. *J Biol Chem* 279(15): 14473-14476.
- Zuris JA, Harir Y, Conlan AR, Shvartsman M, Michaeli D, et al. (2011) Facile transfer of [2Fe-2S] clusters from the diabetes drug target mitoNEET to an apo-acceptor protein. *Proc Natl Acad Sci USA* 108(32): 13047-13052.
- Mittler R, Darash-Yahana M, Sohn YS, Bai F, Song L, et al. (2019) NEET proteins: a new link between iron metabolism, reactive oxygen species, and cancer. *Antioxid Redox Signal* 30(8): 1083-1095.
- Sohn YS, Tamir S, Song L, Michaeli D, Matouk I, et al. (2013) NAF-1 and mitoNEET are central to human breast cancer proliferation by maintaining mitochondrial homeostasis and promoting tumor growth. *Proc Natl Acad Sci USA* 110(36): 14676-14681.
- Kusminski CM, Holland WL, Sun K, Park J, Spurgin SB, et al. (2012) MitoNEET-driven alterations in adipocyte mitochondrial activity reveal a crucial adaptive process that preserves insulin sensitivity in obesity. *Nat Med* 18(10): 1539-1549.
- Chen H, McCaffery JM, Chan DC (2007) Mitochondrial fusion protects against neurodegeneration in the cerebellum. *Cell* 130(3): 548-562.
- De Brito OM, Scorrano L (2008) Mitofusin 2 tethers endoplasmic reticulum to mitochondria. *Nature* 456(7222): 605-610.
- Smirnova E, Griparic L, Shurland DL, Van Der Bliek AM (2001) Dynamin-related protein Drp1 is required for mitochondrial division in mammalian cells. *Mol Biol Cell* 12(8): 2245-2256.
- Geldenhuis WJ, Leeper TC, Carroll RT (2014) MitoNEET as a novel drug target for mitochondrial dysfunction. *Drug Discov Today* 19(10): 1601-1606.
- Furihata T, Takada S, Maekawa S, Tsuda M, Nakahara M, et al. (2021) Cardiac-specific loss of mitoNEET expression is linked with age-related heart failure. *Commun Biol* 4(1): 138.
- Lazarou M, Sliter DA, Kane LA, Sarraf SA, Wang C, et al. (2015) The ubiquitin kinase PINK1 recruits autophagy receptors to induce mitophagy. *Nature* 524(7565): 309-314.
- Narendra DP, Jin SM, Tanaka A, Suen DF, Gautier CA, et al. (2010) PINK1 is selectively stabilized on impaired mitochondria to activate Parkin. *PLoS Biol* 8(1): e1000298.
- Tamir S, Paddock ML, Darash-Yahana-Baram M, Holt SH, Sohn YS, et al. (2015) Structure-function analysis of NEET proteins uncovers their role as key regulators of iron and ROS homeostasis in health and disease. *Biochim Biophys Acta* 1853(6): 1294-1315.
- Martinez A, Sanchez-Martinez A, Pickering JT, Twynning MJ, Murphy LM, et al. (2024) Mitochondrial CISD1/Cisd accumulation blocks mitophagy and genetic or pharmacological inhibition rescues neurodegenerative phenotypes in Pink1/parkin models. *Mol Neurodegen* 19(1): 9.



This work is licensed under Creative Commons Attribution 4.0 License
DOI: [10.19080/AIBM.2026.19.556015](https://doi.org/10.19080/AIBM.2026.19.556015)

Your next submission with Juniper Publishers will reach you the below assets

- Quality Editorial service
- Swift Peer Review
- Reprints availability
- E-prints Service
- Manuscript Podcast for convenient understanding
- Global attainment for your research
- Manuscript accessibility in different formats
(Pdf, E-pub, Full Text, Audio)
- Unceasing customer service

Track the below URL for one-step submission
<https://juniperpublishers.com/online-submission.php>